Lap Time Optimization of a Sports Series Hybrid Electric Vehicle

Roberto Lot and Simos A. Evangelou

***Abstract*—This paper illustrates a methodology for the lap time optimization of a race series hybrid electric vehicle based on the indirect optimal control approach. More specifically, for a vehicle with given characteristics running on a given track, the optimal trajectory and powertrain power flow that minimize the lap time are found. The paper presents a parametric model of a sports series hybrid electric vehicle, illustrates the optimization method and discusses simulation results.**

***Index Terms*—hybrid electric vehicle, vehicle dynamics, optimal control, lap time optimization.**

I. Introduction

HYBRID electric vehicles (HEVs) are becoming more popular due to their potential to address climate change and the demand for a limited, but increasingly expensive, supply of fossil fuels. In addition, a new category of sports and race HEVs is emerging [1], [2]. Although the synergy between multiple energy sources in HEV powertrains is normally used to bring reductions in fuel consumption and noxious emissions, in racing the main interest is about performance and lap time minimization.

In the case of road HEVs various control techniques have been proposed in the literature for the powertrain energy management, ranging from rule-based to optimisation-based [3]–[9]. This paper presents a global optimisation-based control approach that utilises indirect optimal control techniques to optimise not only the powertrain energy flow but also the trajectory of a racing HEV inside a given race circuit. The methodology is established by utilising symbolic dynamic vehicle modelling of appropriate complexity, together with computationally efficient optimal control software [10].

II. Mathematical Model

The powertrain of a Series Hybrid Electric Vehicle (S-HEV) is schematized in Figure 1 and consists of three branches: the spark ignition engine, the battery and the transmission. In driving operating conditions, i.e. while cruising at a constant speed or accelerating, power is request to drive the vehicle. The spark ignition (SI) engine is mechanically connected to the permanent magnet synchronous (PMS) generator, which converts the engine mechanical power P_e into the electric AC power P_g. The rectifier takes this AC power and converts it to DC power P_r, which is provided to the DC link. In the other branch, the battery (possibly) provides additional power P_{bl} to the DC/DC converter, which steps up the battery voltage to v_{dc} and provides power P_b to the DC link. The overall DC link power $P_r + P_b$ is converted from DC into AC by the inverter, which supplies the electric power P_i to the PMS motor. The latter is connected to the wheels by means of a fixed ratio transmission, and the vehicle is finally driven with power P_t. While braking, power is driven through the transmission to recharge the battery. Additionally, mechanical brakes extract power P_h which is transformed into heat and definitively dissipated. Optionally, the battery may be recharged by the SI engine when a power surplus is available. In summary, the S-HEV has three independent power sources, respectively battery P_b, generator P_g and brakes P_h power, that may be variously combined to obtain the desired values of vehicle speed and acceleration. In particular, the battery may conveniently provide boost power while the vehicle is accelerating. However, the battery energy is limited to the value which may be recovered during each lap, hence it is scarse and it is important to use boost effectively and to optimize the whole power management process.

Finally, as a race driver is free to select his preferred trajectory inside the track, to minimize the lap time it is also necessary to optimize the trajectory and speed profile at the same time as optimizing the power flow in the vehicle.

Details of the mathematical model of the S-HEV vehicle and its powertrain, the formulation of the minimum lap time problem and some simulation results are discussed in the next sections.

A. Powertrain

The first power branch (Figure 1) includes the SI engine, the PMS generator and the AC/DC converter. Modelling in detail such elements is not trivial and out of the scope of this work. For the purpose of lap time optimization, the essential feature of this power branch is that the SI engine is not mechanically connected to the vehicle transmission and so it may deliver the maximum available power regardless of the vehicle speed. The total power provided by this branch is found by considering that the SI engine is a source of (limited) power P_e, which is then reduced while flowing through the PMS generator and AC/DC converter, that have efficiencies (assumed constant) η_g and η_r respectively:

$$P_r = \eta_r \eta_g P_e \tag{1}$$

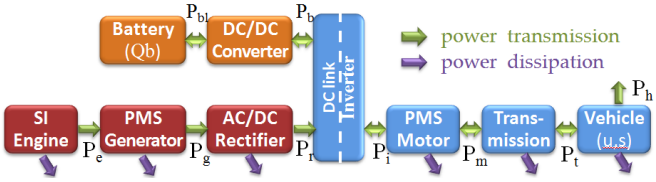

Fig. 1. Powertrain architecture of a Series Hybrid Electric Vehicle (purple arrows indicate power losses).

Manuscript received March 6, 2013; revised April 3, 2013.

R. Lot is with Department of Industrial Engineering, University of Padova, 35100 Padova, Italy e-mail: roberto.lot at unipd.it

S. A. Evangelou is with the Departments of Electrical and Electronic, and Mechanical Engineering, Imperial College London, London, UK e-mail: s.evangelou at imperial.ac.uk

ISBN: 978-988-19252-9-9
ISSN: 2078-0958 (Print); ISSN: 2078-0966 (Online)

The second power branch includes the battery and the DC/DC converter that steps up the low voltage on the battery side to a high voltage on the DC link side. The battery state of charge is described by the following differential equation:

$$\frac{d}{dt}Q_b = -i_b \tag{2}$$

where Q_b is the actual charge and i_b the current of the battery, assumed positive during the discharge phase. Moreover, the battery power (on the low voltage side) is:

$$P_{bl} = i_b v_b \tag{3}$$

where v_b is the closed circuit voltage of the battery, which depends both on the battery charge Q_b and current i_b. Such dependence may be expressed in terms of the electrochemical parameters and an equivalent electrical circuit [11], [12] as follows:

$$v_b = E_b - Ri_b = E_0 + \left(1 - \frac{Q_{max}}{Q}\right) + Ae^{B(Q-Q_{max})} - Ri_b \tag{4}$$

where E_b is the open circuit voltage, R_b is the internal resistance, E_0 is the nominal voltage, Q_{max} is the capacity of the battery, and A, B are two additional constants. The DC/DC converter is simply modelled as a static element having a constant efficiency η_{dc}. Since the converter is bi-directional, the power conversion may be described by means of the following equation:

$$P_b = \eta_{dc}^{\mathrm{sign}(P_b)} P_{bl} \tag{5}$$

where P_b is the battery power on the DC link side. The efficiency is adjusted according to the direction of the power flow, i.e. when the positive power flows from the battery to the DC link $P_b = \eta_{dc} P_{bl}$, on the contrary when the negative power flows from the DC link to charge the battery $P_{bl} = \eta_{dc} P_b$.

Power flow is then collected by the DC link, which drives a bidirectional inverter. Similarly to the rectifier, the inverter is simply modelled by means of a constant efficiency factor η_i, therefore the power balance of the DC link and inverter is described by the following equation:

$$P_i = \eta_i^{\mathrm{sign}(P_r + P_{bl})} (P_r + P_{bl}) \tag{6}$$

where once again the efficiency is adjusted according to the direction of the power flow $\mathrm{sign}(P_r + P_{bl})$. The inverter supplies the electric motor/generator, which is a 3-phase star-connected PMS machine. PMS machines combine a number of attractive features when used in hybrid vehicle applications, such as higher torque-to-inertia ratio and power density than ones of induction or wound-rotor synchronous machines. The dynamic electro-magnetic behaviour of the PMS machine may be effectively described in the rotor $d-q$ reference frame [13] by the following non-linear differential equations:

$$L_q \frac{d}{dt} i_d = v_d - Ri_d + p\omega L i_q \tag{7a}$$

$$L_q \frac{d}{dt} i_q = v_q - Ri_q - p\omega L i_q + \lambda \tag{7b}$$

where i_d, v_d and i_q, v_q are the direct and quadrature components of armature currents and terminal voltages, ω is the rotor angular speed, while the other parameters are described in Table I. Equations (7) model only the power losses due the resistance R of the stator copper windings, while in reality there are other electromagnetic dissipation sources [14] such as Eddy current losses ($\propto \omega^2$) and hysteresis losses ($\propto \omega^2$), while mechanical losses [14] include bearing losses ($\propto \omega$) and windage losses ($\propto \omega^5$). These additional losses are modelled in the dynamic equation of the rotor as follows:

$$J\frac{d}{dt}\omega = \frac{3}{2}p\lambda i_q + T_l + T_d(\omega) \tag{8}$$

where J is the rotor inertia, T_l is the mechanical torque exchanged with the trasmission, and $T_d(\omega)$ is the dissipation torque. The control strategy of the machine [15] uses a null direct current $i_d = 0$. To further simplify the model, it may be observed that the dynamics of electromagnetic phenomena are much faster than mechanical ones, hence transient currents may be neglected. The inertia torque $J\frac{d}{dt}\omega$ is neglected also, as the motor inertia is much smaller than the vehicle inertia to which it is rigidly connected. These assumptions lead to the simplification of differential equations (7), (8) into a set of steady-state algebraic equations, which may be easily solved in term of currents and voltages, leading to the following equation for the input power P_i (exchanged with the inverter) and output power P_m (exchanged with the transmission):

$$P_i = \omega(T_l + T_d) - \frac{2}{3}R\frac{(T_l + T_d)^2}{(p\lambda)^2} \tag{9a}$$

$$P_m = \omega T_l \tag{9b}$$

Equations (9) are capable of describing the reversible PMS machine both when it works as a generator, i.e. with positive power, load torque and quadrature current, or when it works as a motor, i.e. with negative power, load torque and quadrature current. According to such conventions, the PMS efficiency is:

$$\eta_m = \left(\frac{P_m}{P_i}\right)^{\mathrm{sign}(P_i)} \tag{10}$$

and it is reported in Figure 2. The PMS machine efficiency is very high in a wide range of operating condition, even if it is very poor at low speeds, where the resistance losses Ri_q^2 are predominant, and at low torques, where the mechanical losses $\omega T_d(\omega)$ are predominant. The figure also shows the current i_q, which is roughly proportional to the torque, and the overall voltage $\sqrt{v_q^2 + v_d^2}$, which is roughly proportional to the speed. The PMS motor is connected to the transmission and finally to the wheels in a way that the velocity ratio between the motor angular speed ω and the vehicle forward speed v is constant:

$$\tau = \frac{\omega}{u} \tag{11}$$

It is assumed that the transmission has a constant efficiency η_t, the bi-directional power flow is hence modelled with the following equation:

$$P_t = \eta_t^{\mathrm{sign}(P_m)} P_m \tag{12}$$

i.e. when positive power flows form the PMS motor to the vehicle $P_t = \eta_t P_m$, on the contrary when negative power flows from the vehicle to the battery $P_m = \eta_t P_t$.

Brakes are simply modelled as power withdrawal, i.e a source of negative power P_h, which is converted into heat and dissipated.

ISBN: 978-988-19252-9-9
ISSN: 2078-0958 (Print); ISSN: 2078-0966 (Online)

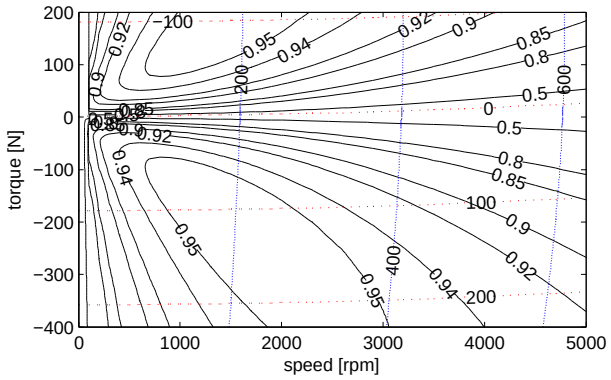

Fig. 2. PMS machine efficiency (solid black), current (horizontal dotted red) and voltage (vertical dotted blue). Positive torques correspond to generator, and negative torques correspond to motor operating conditions.

By coupling and manipulating equations (5), (6), (9), (10), and (12), the vehicle power flow may be completely described as a function of three independent power sources, respectively the generator P_g, battery P_b, and brakes P_h, as follows:

$$P_e = \eta_e^{-1} P_g \tag{13a}$$
$$P_r = \eta_r P_g \tag{13b}$$
$$P_{bl} = \eta_{dc}^{-\operatorname{sign} P_b} P_b \tag{13c}$$
$$P_i = \eta_i^{\operatorname{sign}(\eta_r P_g + P_b)} (\eta_r P_g + P_b) \tag{13d}$$
$$P_t = (\eta_i \eta_m \eta_t)^{\operatorname{sign}(\eta_r P_g + P_b)} (\eta_r P_g + P_b) \tag{13e}$$

The only dynamic variable of the powertrain is the battery charge Q_b, while any other variable may algebraically be expressed as a function of P_g, P_b, P_h.

B. Vehicle and track

This section illustrates the model used to capture the vehicle gross motion on the track for the purpose of trajectory and speed profile optimization. The vehicle is modelled as a single-track rigid body, running on a horizontal flat track (Figure 3). The equations of motion in the longitudinal and

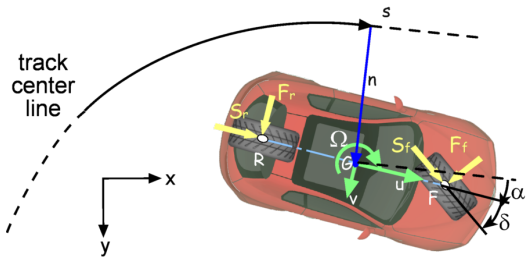

Fig. 3. Single-track vehicle model.

lateral directions are respectively:

$$m\left(\frac{d}{dt}u - \Omega v\right) = S_r + S_f \cos\delta - F_f \sin\delta - F_D \tag{14}$$
$$m\left(\frac{d}{dt}v + \Omega u\right) = F_r + S_f \sin\delta + F_f \cos\delta \tag{15}$$

where m is the vehicle mass, u and v are respectively the longitudinal and lateral speed, Ω is the yaw rate, (S_f, F_f) and (S_r, F_r) are the longitudinal and lateral forces respectively on the front and rear axle, $F_D = \frac{1}{2}\rho C_D A u^2$ is the aerodynamic drag resistance, and δ is the steering angle. The equation for the yaw motion is:

$$I_G \frac{d}{dt}\Omega = aF_f \cos\delta + S_f \sin\delta - bF_r \tag{16}$$

while I_G is the yaw moment of inertia, while a and b are the distance from the vehicle center of gravity (CoG) respectively of the front and rear axle.

Tire longitudinal forces are strictly related to the power flow (13), in particular the propulsive power is transferred to the real axle only, while braking power is distributed on both axle with constant ratio r_b:

$$S_f = \frac{r_b \min(P_t + P_h, 0)}{u} \tag{17a}$$
$$S_r = \frac{P_t + P_h - r_b \min(P_t + P_h, 0)}{u} \tag{17b}$$

where suffixes f and r refer to the front and rear axle.

Vehicle directionality is controlled by means of the steering angle δ. Tire lateral forces are assumed to be proportional to the cornering stiffness K, (small) sideslip angle λ and tire vertical load N as follows:

$$F_f = k_f \lambda_f \simeq K_f \left(\delta - \frac{a\Omega + v}{u}\right) N_f \tag{18a}$$
$$F_r = k_r \lambda_r \simeq K_r \frac{b\Omega - v}{u} N_r \tag{18b}$$

Tire loads are calculated taking into account the load transfer from the front to the rear axle during traction (and vice versa during braking), according to the (approximate) expressions:

$$N_r = \frac{a}{a+b} mg + \frac{h}{a+b}(S_r + S_f) \tag{19a}$$
$$N_f = \frac{b}{a+b} mg - \frac{h}{a+b}(S_r + S_f) \tag{19b}$$

where h is the vehicle center of gravity height. The track is assumed to be flat and to lay on the horizontal plane xy. The curvature Θ of the track reference line Γ may be calculated from its cartesian coordinates (x, y) as a function of the travelled space s as follows:

$$\Theta(s) = \sqrt{\left(\frac{d^2x}{ds^2}\right)^2 + \left(\frac{d^2y}{ds^2}\right)^2} \tag{20}$$

To add the second dimension of the strip-like track model it is sufficient to specify the distance from the borders, which possibly depends on the position s. To track the position and orientation of the vehicle, it is very convenient to use the triple of curvilinear coordinates (s, n, α), where s and n are respectively the longitudinal and lateral position on the road strip and α is the vehicle heading relative to the road. As depicted in Figure 3, such coordinates are related to the vehicle speeds by the following differential relations:

$$\frac{d}{dt}s = \frac{u\cos\alpha - v\sin\alpha}{1 - n\,\Theta(s)} \tag{21a}$$
$$\frac{d}{dt}n = u\sin\alpha + v\cos\alpha \tag{21b}$$
$$\frac{d}{dt}\alpha = \Omega - \frac{u\cos\alpha - v\sin\alpha}{1 - n\,\Theta(s)}\Theta(s) \tag{21c}$$

In conclusion, sections II-A and II-B describe the power train flow and the vehicle gross motion as a function of 7 variables $\boldsymbol{x}(t) = \{Q_b, u, v, \Omega, s, n, \alpha\}^T$ and 4 control inputs $\boldsymbol{u}(t) = \{P_g, P_b, P_h, \delta\}^T$.

ISBN: 978-988-19252-9-9
ISSN: 2078-0958 (Print); ISSN: 2078-0966 (Online)

TABLE I
MODEL PARAMETERS

Symbol	Value	Parameter
m	1050 kg	vehicle mass
h	0.450 m	center of gravity (CoG) height
a	1.150 m	CoG to front axle
b	1.000 m	CoG to rear axle distancee
I_z	800 kg m^2	yaw moment of inertia
$\frac{1}{2}\rho C_D A$	0.378 kg/m	aerodynamic drag factor
K_r, K_f	20 rad^{-1}	tires non-dimensional sideslip stiffness
μ_r, μ_f	1.05	tires friction coefficient
r_b	0.60	braking torque ratio on the front axle
$P_{e,max}$	125 kW	SI engine max power
E_0	200 V	battery nominal voltage
Q_{max}	10 Ah	battery capacity
$i_{b,d}$	100 A	battery max discharging current
$i_{b,c}$	50 A	battery max recharging current
R_b	0.200 Ω	Battery internal resistance
v_{dc}	1000 V	DC link voltage
p	6	number of pole pairs of the PMS motor
R	0.040 Ω	PMS stator resistance
L_d, L_q	450 mH	stator inductances of PMS motor
λ	0.20 Wb	rotor magnetic flux of PMS motor
$i_{m,max}$	250 A	max current of PMS motor
τ	9	transmission ratio
η_r	0.96	rectifier efficiency
η_{dc}	0.96	DC/DC converter efficiency
η_i	0.96	inverter efficiency
η_t	0.85	transmission efficiency (tires included)

III. THE MINIMUM LAP TIME PROBLEM

The minimum lap time problem consists in finding the vehicle control inputs that minimize the time T necessary to move the vehicle from the starting line to the finish one of the given track, by satisfying the mechanical equations of motion as well as inequality constraints such as tires adherence, max power, track width, etc. As the final value T of the time variable t is clearly undefined, while the curvilinear abscissa s varies from between fixed initial point $s = 0$ and end point $s = L$, it is convenient to mathematically formulate the problem in terms of the independent variable s instead of t. Such optimal control problem (OCP) may be formulated as follows:

$$\text{find:} \quad \min_{\boldsymbol{u}\in\boldsymbol{U}} T \tag{22a}$$

$$\text{subject to:} \quad \frac{d}{ds}\boldsymbol{x} = \boldsymbol{f}\left(\boldsymbol{x}, \boldsymbol{u}, s\right) \tag{22b}$$

$$\boldsymbol{\psi}\left(\boldsymbol{x}, \boldsymbol{u}, s\right) \leq \boldsymbol{0} \tag{22c}$$

$$\boldsymbol{b}\left(\boldsymbol{x}(0), \boldsymbol{x}(L)\right) = \boldsymbol{0} \tag{22d}$$

where $\boldsymbol{x}$ and $\boldsymbol{u}$ are respectively the state variables and inputs vector, (22b) is the state space model in the s domain, (22c) are algebraic inequalities that may bound both the state variables and control inputs and (22d) is the set of boundary conditions used to (partially) specify the vehicle state at the beginning and at the end of the maneuver.

A. State space model

The vehicle model described in Sections II-A and II-B has to be slightly modified to take into account that in the OCP formulation (22) it is allowed to bound the controls $\boldsymbol{u}$, but it is not possible to guarantee that such controls remain smooth and to avoid unrealistic jerky maneuvers. For this reason, powers and steering angle are not controlled directly, but via their (bounded) time derivative, as follows:

$$\frac{d}{dt}\delta = \omega_\delta \tag{23a}$$

$$\frac{d}{dt}P_g = mu\, j_g \tag{23b}$$

$$\frac{d}{dt}P_h = mu\, j_b \tag{23c}$$

$$\frac{d}{dt}P_w = mu\, j_h \tag{23d}$$

where power controls j have dimensions of jerk [ms^{-3}].

To be consistent with the OCP formulation (22b), the independent variable t must be replaced with the new independent variable s in all model equations, according to the following derivation rule:

$$\boldsymbol{x'} = \frac{d\boldsymbol{x}}{ds} = \frac{d\boldsymbol{x}}{dt}\frac{dt}{ds} = \frac{d\boldsymbol{x}}{dt}\, t' \tag{24}$$

where the time variation with respect to the track length is simply calculated by inverting the relation (21a) as follows:

$$t' = \frac{1 - n\,\Theta(s)}{u\cos\alpha - v\sin\alpha} \tag{25}$$

At this point the s-domain state space model has 11 state variables:

$$\boldsymbol{x}(s) = \{t, Q_b, u, v, \Omega, n, \alpha, P_g, P_b, P_h, \delta\}^T \tag{26}$$

and 4 inputs:

$$\boldsymbol{u}(s) = \{\omega_\delta, j_g, j_b, j_h\}^T \tag{27}$$

B. Inequality constraints and boundary conditions

Inequalities (22c) are used to keep the vehicle operating conditions inside their admissible range. Power train constraints include the limitation of the SI engine power:

$$0 \leq P_e \leq P_{e,max} \tag{28}$$

The battery is constrained in terms of charge and current:

$$Q_{b,min} \leq Q_b \leq Q_{b,max} \tag{29a}$$

$$-|i_{b,d}| \leq i_b \leq |i_{b,c}| \tag{29b}$$

The PMS motor/generator is constrained in terms of voltage- and current:

$$v_d^2 + v_q^2 \leq \frac{v_{dc}^2}{3} \tag{30a}$$

$$|i_q| \leq i_{m,max} \tag{30b}$$

Braking power is constrained to be negative:

$$P_h \leq 0 \tag{31}$$

The vehicle must remain inside the track borders:

$$-(b_l - w) \leq n \leq b_r - w \tag{32}$$

while w is the vehicle width and b_l, b_r are the left and right borders distance.

Tires adherence is constrained inside their *traction ellipse*:

$$F_r^2 + S_r^2 \leq \left(\mu_r N_r\right)^2 \tag{33a}$$

$$F_f^2 + S_f^2 \leq \left(\mu_f N_f\right)^2 \tag{33b}$$

ISBN: 978-988-19252-9-9
ISSN: 2078-0958 (Print); ISSN: 2078-0966 (Online)

where μ_r, μ_r are the friction coefficients respectively for the rear and front tire.

To complete the problem definition it is necessary to specify boundary conditions (22d). As the optimization is made on a closed loop track, it is natural to impose cyclic boundary conditions for all state variables $\boldsymbol{x}(s)$, except for the time t - which is obviously acyclic.

C. Solution of the Minimum Lap Time problem

The optimal control problem defined in equations (22) may be solved by using various methods [16], such as non linear programming, dynamic programming or indirect methods. The latter approach has been used in this work. Summarizing, the inequality constraints (22c) have been replaced with some (approximately) equivalent terms in the penalty function (22a) by means of a wall function W which is null when the constraint is satisfied and becomes very large as the boundary is approached and possibly exceeded. Moreover, the presence of equality constraints (22b) is managed with the Lagrange's multiplier methods. In this manner, the constrained OCP problem (22) is converted into the equivalent, unconstrained minimization of the following functional:

$$J(\boldsymbol{x}, \boldsymbol{u}, s) = t(L) + \sum_j \int_0^L W(\psi_j) ds + \sum_i \int_0^L \gamma_i (x_i' - f_i) ds \tag{34}$$

To minimize $J(\cdot)$, the first variation principle is used and the minimization problem is finally converted into a differential boundary value problem (BVP). More details are given in [10], [17]. Since this process heavily requires the manipulation of the equations of motion at symbolically level, the whole problem formulation has been carried out in Maple [18]. In particular the mathematical model of the vehicle has been modelled by using the MBSymba package [19], then the OCP problem has been formulated by using the XOptima package, which also automatically generates C++ code ready to be compiled. Finally, the numerical integration of the BVP problem is performed by using the specialized solver described in [10].

IV. Simulation Results

Simulations have been carried out for the exemplary HEV vehicle, whose characteristics are summarized in table I, and the Mugello circuit. Figure 4 shows the circuit and also the calculated optimal trajectory, speed and acceleration. In order to better understand the significance of the battery power boost and its optimal utilization, the vehicle performances with and without the battery are compared. The figure highlights that the boost (blue line) slightly increases acceleration and top speed, leading to a difference in the lap time of 189.19 s versus 191.24 s (i.e. +2.05 s) when the battery is disabled. Secondly, the figure shows that speed and acceleration are equal both at the beginning and at the end of the lap, according to the imposed cyclic boundary conditions. While acceleration is limited by engine battery power, deceleration is limited by tire adherence. The latter is depicted in Figure 5 in terms of the lateral force to tire load ratio vs longitudinal force to tire load ratio, for both tires. In particular this picture shows that the optimal maneuver makes large utilization of combined longitudinal and lateral

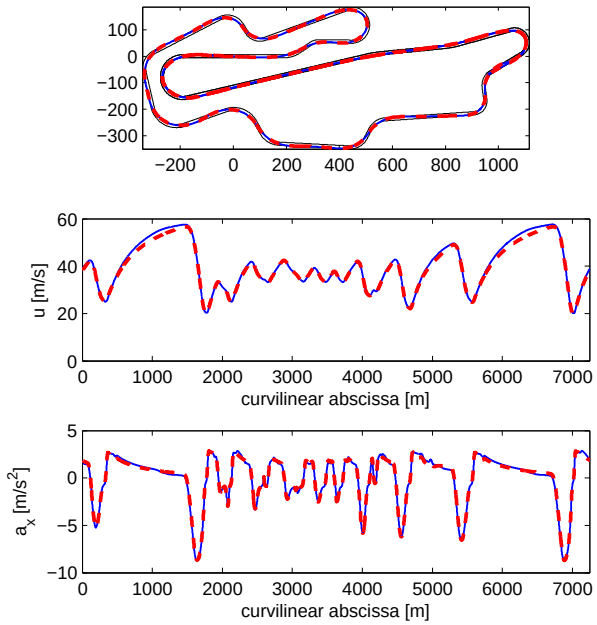

Fig. 4. Lap time optimization at the Mugello circuit: optimal trajectory, speed and longitudinal acceleration (solid blue: reference HEV vehicle, dashed red: battery disabled).

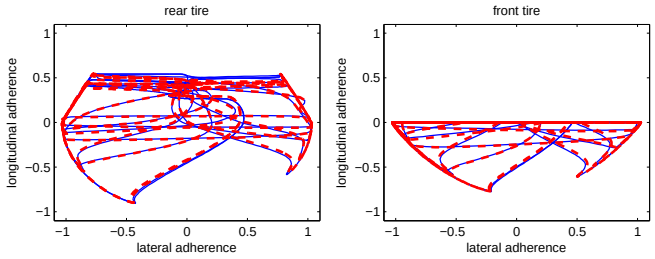

Fig. 5. Adherence of the rear and front tires (solid blue: reference HEV vehicle, dashed red: battery disabled).

forces, as only race drivers do. Figure 6 highlights the vehicle power flow from the spark ignition engine and battery to the PMS motor/generator. During acceleration, the SI engine is capable of providing the maximum power regardless of the vehicle speed, indeed the engine may easily operate at the speed of maximum power thanks to the absence of any mechanical coupling between the engine and the traction axle. The battery presents a more evident on/off operational mode, approximately switching from the positive maximum of delivered power to the negative maximum of recharge power. As it is required that the battery state of charge (SoC) at the end of the lap should be equal to the beginning (as depicted in figure 7), the integral of battery power is slightly negative to counterbalance power train losses. It may be observed that the battery is recharged not only by recovering energy during braking, but also by using the SI engine power when there is some surplus (e.g. at s=3000 m) and even during acceleration (e.g. $1250 \lesssim s \lesssim 1500$, $6500 \lesssim s \lesssim 6800$, etc.). This effect is more evident by analyzing the PMS power: the maximum battery power is used to boost the acceleration from $s = 400$ m (blue line vs red line), at $s = 1020$ m the battery boost is not more used because the energy stored in the battery is not more sufficient. From $s = 1180$ m, the reference case highlights that the full available SI engine power is not provided to the PMS motor

ISBN: 978-988-19252-9-9
ISSN: 2078-0958 (Print); ISSN: 2078-0966 (Online)

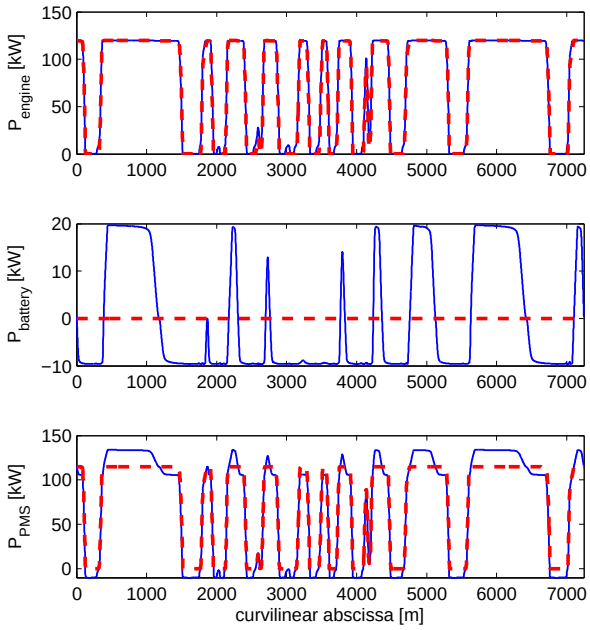

Fig. 6. Power of the SI engine, battery and PMS motor/generator (solid blue: reference HEV vehicle, dashed red: battery disabled).

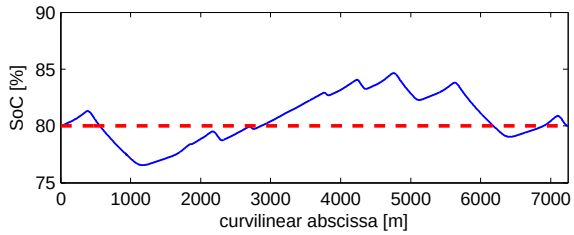

Fig. 7. Battery State of Charge (solid blue: reference HEV vehicle, dashed red: battery disabled).

(as in the case of disabled battery), but it is split between the motor and the battery. In other words, to minimize the lap time, it is convenient to use the battery to boost during the initial phase of the acceleration, even if it is necessary to relinquish some propulsive power in the successive phase to recharge the battery. The proper timing of battery boost and recharging (shown in figure 7) is hence crucial for the lap time minimization. This task is excellently carried out with the global optimization approach adopted, while it would be very difficult to optimally manage the power flow by means of some pre-determinate control strategy.

V. Conclusions

This paper illustrates a methodology for the lap time optimization of a race series hybrid electric vehicle based on the indirect optimal control approach. This method is very powerful because it does not require the definition of a specific control architecture or strategy in advance, while system inputs are given as a result of the optimization process. Second, the optimization is performed *globally*, i.e along the whole track. This is essential in this kind of problem, where the battery introduces a strong coupling among the different sections of the circuit: battery boost may be used while exiting from a curve only if the battery has been recharged while braking in another section, not necessarily close to the first one.

Conversely, the indirect method is not so popular due to the difficulties associated with the problem implementation as well as the numerical solution. The transformation of the constrained optimization problem into an equivalent boundary value problem (BVP) requires the definition of an optimization-tailored model and the symbolic manipulation of the model equations, that in the present work have been performed by using computer symbolic algebra tools. This approach also leads to very computationally efficient applications, with the optimizations in this paper carried out in times much faster than real time, highlighting that this approach may be applied effectively to more complex vehicle models as well.

References

[1] S. Lambert, S. Maggs, P. Faithfull, and A. Vinsome, "Development of a hybrid electric racing car," in *Hybrid and Eco-Friendly Vehicle Conference, 2008. IET HEVC 2008*, Dec., pp. 1–5.

[2] http://www.bbc.co.uk/sport/0/formula1/20640255, "How Formula 1 is going green for 2014."

[3] F. R. Salmasi, "Control strategies for hybrid electric vehicles: evolution, classification, comparison, and future trends," *IEEE Trans. Veh. Technol.*, vol. 56, no. 5, pp. 2393–2404, September 2007.

[4] D. A. Crolla, Q. Ren, S. ElDemerdash, and F. Yu, "Controller design for hybrid vehicles – state of the art review," in *Vehicle Power and Propulsion Conference, 2008. VPPC '08. IEEE*, sept. 2008, pp. 1 –6.

[5] X. He, M. Parten, and T. Maxwell, "Energy management strategies for a hybrid electric vehicle," in *Vehicle Power and Propulsion, 2005 IEEE Conference*, sept. 2005, pp. 390 – 394.

[6] C. Musardo, G. Rizzoni, and B. Staccia, "A-ECMS: An adaptive algorithm for hybrid electric vehicle energy management," in *Decision and Control, 2005 and 2005 European Control Conference. CDC-ECC '05. 44th IEEE Conference on*, dec. 2005, pp. 1816 – 1823.

[7] L. V. Pérez and E. A. Pilotta, "Optimal power split in a hybrid electric vehicle using direct transcription of an optimal control problem," *Math. and Comput. in Simulation*, vol. 79, no. 6, pp. 1959–1970, 2009.

[8] L. Serrao, S. Onori, and G. Rizzoni, "ECMS as a realization of Pontryagin's minimum principle for HEV control," in *American Control Conference, 2009. ACC '09.*, june 2009, pp. 3964 –3969.

[9] S. Stockar, V. Marano, M. Canova, G. Rizzoni, and L. Guzzella, "Energy-optimal control of plug-in hybrid electric vehicles for real-world driving cycles," *Vehicular Technology, IEEE Transactions on*, vol. 60, no. 7, pp. 2949–2962, September 2011.

[10] E. Bertolazzi, F. Biral, and M. Da Lio, "Symbolic-numeric efficient solution of optimal control problems for multibody systems," *Journal of Computational and Applied Mathematics*, vol. 185, no. 2, pp. 404–421, 2006.

[11] C. M. Shepherd, "Design of primary and secondary cells - part 2. an equation describing battery discharge," *Journal of Electrochemical Society*, vol. 112, pp. 657–664, July 1965.

[12] O. Tremblay and L. A. Dessaint, "Experimental validation of a battery dynamic model for ev applications," *World Electric Vehicle Journal*, vol. 3, 2009.

[13] P. Pillay and R. Krishnan, "Modelling, simulation, and analysis of permanent-magnet motor drives, Part I: The permanent-magnet synchronous motor drive," *IEEE Transactions on Industry Application*, vol. 25, no. 2, pp. 265–273, 1989.

[14] J. Hey, D. A. Howey, R. Martinez-Botas, and M. Lamperth, "Transient thermal modeling of an axial flux permanent magnet (AFPM) machine using a hybrid thermal model," *International Conference on Fluids and Thermal Engineering*, 2010.

[15] S. Morimoto, Y. Takeda, T. Hirasa, and K. Taniguchi, "Expansion of operating limits for permanent magnet motor by current vector control considering inverter capacity," *Industry Applications, IEEE Transactions on*, vol. 26, no. 5, pp. 866 –871, sep/oct 1990.

[16] A. E. Bryson, *Dynamic optimization*. Addison Wesley, 1999.

[17] V. Cossalter, M. Da Lio, R. Lot, and L. Fabbri, "A general method for the evaluation of vehicle manoeuvrability with special emphasis on motorcycles," *Vehicle System Dynamics*, vol. 31, no. 2, pp. 113–135, 1999.

[18] www.maplesoft.com, "Maple."

[19] R. Lot and M. Da Lio, "A symbolic approach for automatic generation of the equations of motion of multibody systems," *Multibody System Dynamics*, vol. 12, no. 2, pp. 147–172, 2004.

ISBN: 978-988-19252-9-9
ISSN: 2078-0958 (Print); ISSN: 2078-0966 (Online)